

文章编号:1001-9014(2023)04-0476-07

DOI:10.11972/j. issn. 1001-9014. 2023. 04. 008

基于银/碳纳米颗粒近红外驱动的大调制深度太赫兹调制器

苟晗光¹, 朱宇¹, 邬宗冬¹, 史光华², 赖伟恩^{1*}

(1. 合肥工业大学 仪器科学与光电工程学院 光电技术研究院 特种显示技术国家重点实验室 测量理论与精密仪器安徽省重点实验室,安徽 合肥 230009;
2. 中国电子科技集团 第13研究所,河北 石家庄 050051)

摘要:近红外光驱动的太赫兹调制器是太赫兹/红外光纤混合通信系统中的重要组成部分。这里提出了一种基于银纳米颗粒/碳量子点(Ag NPs/CDs)近红外驱动的太赫兹调制器。实验结果表明,银纳米颗粒(Ag NPs)与碳量子点(CDs)的结合会引起纳米颗粒的量子尺寸效应和介电限域效应,利用Ag NPs/CDs可以增强硅基底对近红外光的吸收,从而实现近红外驱动的太赫兹波调制。通过808 nm的近红外调制激励源,对样品进行了0.22~0.33 THz范围内的太赫兹透射特性的表征,与参考硅基片相比,Ag NPs/CDs近红外太赫兹调制器的调制深度可以达到83%左右,显著高于参考硅基片的调制深度(~54%),实现了大调制深度的太赫兹波调制。本研究工作在太赫兹/红外光纤混合通信系统中拥有重要的应用价值。

关 键 词:太赫兹; 纳米颗粒; 太赫兹调制器; 近红外光调制; 表面等离子体共振

中图分类号:TN29 **文献标识码:**A

NIR-driven large modulation depth terahertz modulator based on silver/carbon nanoparticles

GOU Han-Guang¹, ZHU Yu¹, WU Zong-Dong¹, SHI Guang-Hua², LAI Wei-En^{1*}

(1. National Engineering Laboratory of Special Display Technology, National Key Laboratory of Advanced Display Technology, Anhui Province Key Laboratory of Measuring Theory and Precision Instrument, Academy of Optoelectronic Technology, School of Instrument Science and Optoelectronics Engineering, Hefei University of Technology, Hefei 230009, China;
2. The 13th Research Institute of China Electronics Technology Group, Shijiazhuang 050051, China)

Abstract: Near-infrared light-driven terahertz modulators are an important component in terahertz/infrared fiber-optic hybrid communication systems. Here, a near-infrared driven terahertz modulator based on silver nanoparticles/carbon quantum dots (Ag NPs/CDs) is proposed. Experimental results show that the combination of silver nanoparticles (Ag NPs) and carbon quantum dots (CDs) induces quantum size effect and dielectric confinement effect of nanoparticles, and the absorption of NIR light by silicon substrate can be enhanced by using Ag NPs/CDs to achieve NIR-driven terahertz wave modulation. The terahertz transmission characteristics of the sample were characterized in the range of 0.22~0.33 THz with the 808 nm NIR modulation excitation source, and the modulation depth of the Ag NPs/CDs NIR terahertz modulator could reach about 83% compared with the reference silicon substrate, which was significantly higher than the modulation depth of the reference silicon substrate (~54%), realizing the terahertz wave modulation with large

收稿日期:2022-12-09,修回日期:2023-01-15

Received date:2022-12-09, revised date:2023-01-15

基金项目:安徽高校协同创新项目(No. GXXT-2022-015);中央高校基本科研业务费(No. PA2021GDSK0098);德国科学基金(Deutsche Forschungsgemeinschaft);德国研究基金会(Deutsche Forschungsgemeinschaft),DFG: RA2841/12-1-Grant No. /Projektnummer 456700276),以及中国-德国科学研究中心;中德研究促进中心(CDZ)中德研究促进中心,GZ1580)的框架内。功能-纳米-材料-科学合作小组"FNMS-COOP"

Foundation items: The University Synergy Innovation Program of Anhui Province (No. GXXT-2022-015); Fundamental Research Funds for the Central Universities of China (No. PA2021GDSK0098); the Deutsche Forschungsgemeinschaft (German Research Foundation, DFG: RA2841/12-1-Grant No. /Projektnummer 456700276), and the Chinesisch-Deutsches Zentrum für Wissenschaftsförderung (Sino-German Center for Research Promotion, CDZ: Grant No. GZ1580) within the frame of the Functional-Nano-Materials-Sciences Cooperation Group "FNMS-COOP"

作者简介(Biography):赖伟恩(1986—),男,福建龙岩人,博士,副教授,2014年于电子科技大学获得博士学位,主要从事红外/太赫兹功能器件及光谱技术研究。E-mail:wnlai@hfut.edu.cn

***通讯作者(Corresponding author):** E-mail: wnlai@hfut.edu.cn

modulation depth. This research work has important applications in terahertz/infrared fiber hybrid communication systems.

Key words: terahertz, nanoparticles, terahertz modulator, near-infrared light modulation, surface plasmon resonance

引言

近年来,位于微波和红外辐射之间的太赫兹波,因其独特的穿透性、安全性、高频率等性质,在成像、国防安全、生物样品检测和无线通信等领域得到了广泛的应用^[1-6]。这些应用所涉及的太赫兹系统中,太赫兹调制器主要用于调控太赫兹波的电磁特性。通过外部激励,如光、热、电等,来调控太赫兹波的相位、幅度、极化状态等特性^[7-12]。与热激励和电激励相比,光控调制器对材料、工作环境和工艺要求较低,因此太赫兹调制器常用光激励调制^[13]。激光照射在半导体材料表面产生光生载流子,引起材料电导率的改变,太赫兹波的透射率和反射率也随之改变,从而实现对太赫兹波的调制^[14]。硅作为太赫兹波段常用的基底材料,在太赫兹调制器中得到了广泛的应用^[15]。但是,硅基底自身光吸收较弱,很难获得较高的调制深度,这一点极大地制约了硅基底太赫兹调制器的性能^[16]。

为了增强硅基底的光吸收,提高太赫兹调制器的性能,对新材料、新方法提出了更高要求,纳米材料因为其独特的尺寸效应成为了提高硅基底光吸收的理想材料^[17]。长期以来,基于金属纳米材料的调制器被广泛关注。例如,Wen等人^[18, 19]提出了基于Au球形纳米颗粒和Au纳米棒的硅基太赫兹调制器,基于Au纳米粒子的局域等离子体共振,在光激发下产生局域电场增强,实现对太赫兹波的调制。Zhou等人^[20]使用金属纳米棒(GNRs)与硅基材料集成,提高了太赫兹调制性能。Yu等人^[21]通过银纳米棒的等离子体热载流子效应,使得光激发电子更容易跳出势垒,组装在PVA和硅之间的异质结构中增强了太赫兹的全光调制。然而传统金属纳米颗粒的吸收光谱主要集中在可见光范围,且吸收范围极窄,难以满足近红外与太赫兹混合通信系统的要求。Lai等人^[22]通过多次迭代合成大尺寸Ag NPs实现了近红外波段的太赫兹调制器,但其制备复杂,不适合实际应用。为了克服传统金属纳米颗粒制备复杂,近红外光吸收差,吸收范围窄等诸多缺点,实现近红外光驱动的太赫兹调制器的应用,对近红外光吸收的纳米颗粒太赫兹调制器的研究就显得尤为重要。

碳量子点(CDs)的介电常数与金属纳米颗粒有较大差别,这使得CDs具有优异的光电性能,在生物成像、生物传感器^[23, 24]、催化剂^[25]、光电器件^[26, 27]及能量器件^[28, 29]的应用中发挥着重要作用。本文提出了一种基于银纳米颗粒/碳量子点(Ag NPs/CDs)近红外驱动的太赫兹调制器。通过将CDs与Ag NPs相结合的方法得到Ag NPs/CDs结构,改变了纳米粒子原有的介电环境,使得Ag NPs/CDs在近红外波段获得了更好的吸收光谱。Ag NPs/CDs的近红外驱动的太赫兹调制器不仅保留了Ag NPs优异的消光系数,又可以实现在近红外波段的太赫兹调制,同时也具有制备简单的优点。

1 实验描述

实验选取3 mg水溶性的碳量子点(CDs),溶解于1 ml去离子水中;将CDs溶液在室温下搅拌约15 min,得到CDs溶液。1 mg硝酸银(AgNO₃)溶于1 ml去离子水中;将AgNO₃溶液加入CDs溶液中,室温下搅拌15 min,在254 nm紫外光照射15 min下制备成银纳米颗粒/碳量子点(Ag NPs/CDs)共混溶液。超声清洗硅片,并用氮气将硅片吹干,置于热台上。然后取适量合成所得的Ag NPs/CDs溶液,滴涂于硅片的中心区域,55 °C加热至溶剂蒸发,制备得到Ag NPs/CDs近红外驱动的太赫兹调制器。

太赫兹波的调制实验采用了矢量网络分析仪(VNA)(Keysight Technologies, Inc., Santa Rosa, CA, USA)和两台毫米波扩频模块(Virginia Diodes, Inc. Charlottesville, VA, USA),使用808 nm波长的近红外激光器作为外部激励源。将参考硅基片和银纳米颗粒/碳量子点(Ag NPs/CDs)近红外驱动的太赫兹调制器分别置于样品夹上,然后调控激光器功率,采集不同功率下该器件的太赫兹辐射调制性能数据。

2 结果与讨论

2.1 银纳米颗粒/碳量子点(Ag NPs/CDs)的表征

为了探究Ag NPs/CDs的结构特性,对紫外光线下合成的Ag NPs/CDs进行了透射电子显微镜(TEM)表征。**图1(a)**展示了Ag NPs/CDs的三维结构示意图,其中具有银白色金属质感的大颗粒为Ag

NPs, 灰色小颗粒为CDs, CDs悬挂在Ag NPs表面形成了Ag NPs/CDs结构。Ag NPs/CDs分布情况的TEM表征如图1(c)所示, 所得的Ag NPs/CDs颗粒的尺寸大小均匀, 分散性良好, 图中大颗粒表示Ag NPs, 其中小颗粒为CDs, 从图中观察可知CDs依附在Ag NPs表面, 共同形成Ag NPs/CDs。图1(b)和(d)则反映了Ag NPs/CDs颗粒的粒径分布情况, 图1(b)为Ag NPs的粒径分布情况, 图1(d)为CDs的粒径分布情况, 从统计图中可以看到CDs的平均粒径为2.65 nm; Ag NPs的平均粒径为14.26 nm, 这也与参考文献中描述的碳量子点与银纳米颗粒的粒径尺寸近似^[30–35]。两种粒径分布趋势分别对应图中红线所示, CDs和Ag NPs的粒径分布都很好地符合了正态分布。通过对Ag NPs/CDs的表征, 明确了Ag NPs/CDs的几何结构, 即CDs悬挂包覆在Ag NPs表面, 两者共同形成Ag NPs/CDs结构。

2.2 银纳米颗粒/碳量子点的光谱分析和电场分布研究

为了更好地展示Ag NPs/CDs在近红外波段的光吸收现象, 我们使用紫外可见分光光度计(UV-

Vis)对CDs溶液、Ag NPs溶液和Ag NPs/CDs溶液的吸收光谱范围进行了对比测试, 结果如图2(a)所示。图中蓝紫色实线为CDs的UV-Vis吸收光谱, 可以看到CDs的吸收光谱主要集中在342 nm附近, 当入射光波长超过450 nm的截止波长时, CDs对光的吸收几乎可以忽略不计; Ag NPs颗粒吸收光谱如浅绿色实线所示, 在808 nm近红外光的吸收只有0.01左右; Ag NPs/CDs的UV-Vis吸收光谱如红色实线所示, 从图中可知Ag NPs/CDs的吸收光谱几乎包含了从紫外到近红外的整个光谱范围, 其截止波长位于850 nm处, 不难发现相较于CDs和Ag NPs, Ag NPs/CDs拥有更宽的吸收光谱范围, 且Ag NPs/CDs在近红外波段拥有更好的光吸收效果。图2(b)为相应溶液的图片, 图中左侧为CDs溶液, 右侧为Ag NPs/CDs溶液, 可以看到CDs溶液沉积银后溶液由棕黄色变为浅橙色。

此外, 为了更好地说明Ag NPs/CDs结构对硅基底光吸收的影响, 使用有限元时域差分法(FDTD)对银纳米颗粒/碳量子点(Ag NPs/CDs)近红外驱动的太赫兹调制器进行了模拟。图2(c)展示了Ag NPs/

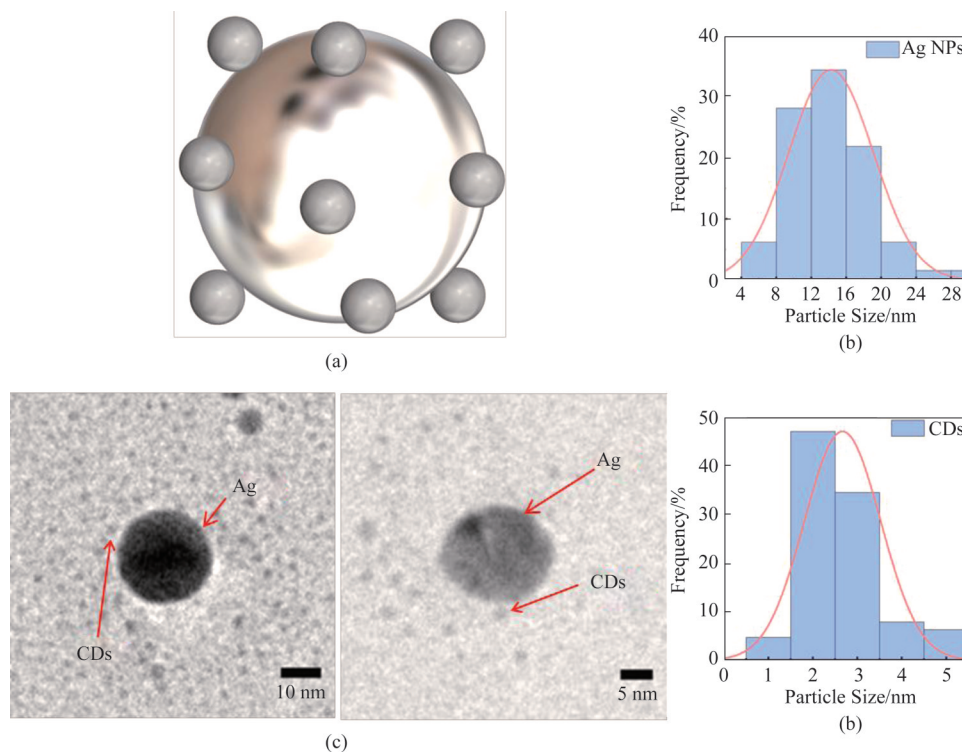


图1 (a)紫外光照下合成Ag NPs/CDs的三维模型,(b)Ag NPs纳米颗粒对应的粒径分布图,(c)Ag NPs/CDs的TEM图,(d)CDs纳米颗粒对应的粒径分布图

Fig. 1 (a) Three-dimensional model for the synthesis of Ag NPs/CDs under UV illumination, (b) particle size distribution map corresponding to Ag NPs nanoparticles, (c) TEM map of Ag NPs/CDs, (d) particle size distribution map corresponding to CDs nanoparticles

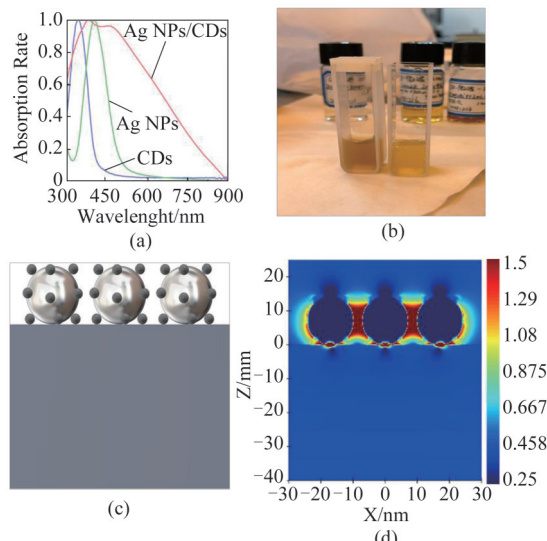


图2 (a)Ag NPs/CDs与CDs和Ag NPs的UV-Vis吸收光谱对比图,(b)CDs(左)和Ag NPs/CDs(右)的相应溶液图片,(c)Ag NPs/CDs调制器结构模型图,(d)808 nm近红外光照射下,Ag NPs/CDs调制器的电场分布

Fig. 2 (a) UV-Vis absorption spectra of Ag NPs/CDs compared with CDs and Ag NPs, (b) corresponding solutions of CDs (left) and Ag NPs/CDs (right), (c) structure model of Ag NPs/CDs modulator, (d) electric field distribution of Ag NPs/CDs modulator under near infrared irradiation at 808 nm

CDs调制器的结构模型,其中Ag NPs/CDs模型的几何参数与TEM表征得到的几何参数一致,CDs与Ag NPs为粒径均匀的球形颗粒,CDs悬挂包覆在Ag NPs的表面,并将其理想化分布在硅基底表面的规则阵列内。在仿真中,使用808 nm近红外光作为光源,为了得到精确的电场分布情况,在纳米颗粒与硅表面区域采用了0.01 nm的细分网格,得到的Ag NPs/CDs界面处的电场分布情况如图2(d)所示。可以看出,在808 nm近红外激光的照射下,Ag NPs/CDs周围呈现出明显的电场增强。

通过对银纳米颗粒/碳量子点的吸收光谱以及表面电场分布的分析,我们把Ag NPs/CDs近红外吸收增强归因于量子尺寸效应和介电限域效应。首先,通过图1(b)可知CDs悬挂包覆在Ag NPs表面,这使得纳米颗粒的直径发生了明显的增大^[36],粒径的增加使得Ag NPs/CDs的共振吸收波长明显红移。其次,在近红外波段银的介电常数(-31.69)是碳的介电常数(5.78)的5.5倍,根据Takagahara^[37]提出的有效质量近似法,两种材料介电常数相差越大,介电限域效应就越强,其在近红外波段的吸收光谱就越强,这也与参考文献描述相符^[38-40]。因此,通过

Ag NPs/CDs的尺寸效应和介电限域效应,Ag NPs/CDs调制器可以很好地将近红外光耦合在Ag NPs/CDs结构中,使得硅基底表面产生局域性电场,并导致其光吸收增强。

2.3 银纳米颗粒/碳量子点的光调制太赫兹波传输特性分析

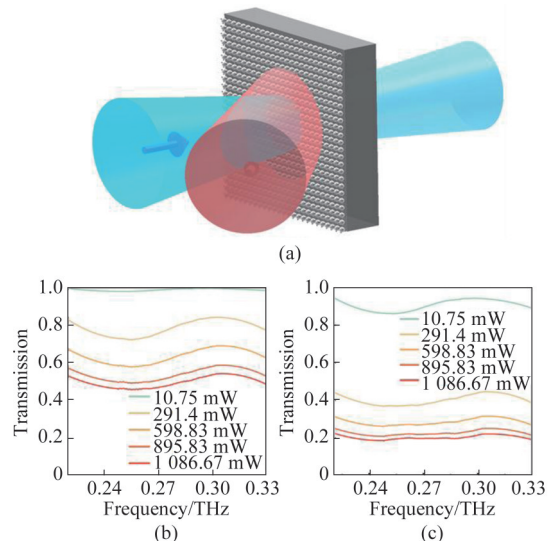


图3 (a)808 nm激光调制Ag NPs/CDs调制器的太赫兹实验示意图,在不同功率的激光辐射调制下,太赫兹波透过(b)参考硅片和(c)Ag NPs/CDs调制器的归一化太赫兹波透过率

Fig. 3 (a) The schematic diagram of terahertz experiments with 808 nm laser modulation of Ag NPs/CDs modulator, terahertz wave transmission under laser radiation modulation with different powers, (b) reference silicon wafer and (c) normalized terahertz wave transmission of Ag NPs/CDs modulator

为了更好地展示Ag NPs/CDs近红外驱动的太赫兹调制器的调制效果,对Ag NPs/CDs近红外驱动的太赫兹调制器在0.22~0.33 THz波段进行了太赫兹传输特性测试。图3(a)为Ag NPs/CDs调制器在808 nm近红外激光调制下0.22~0.33 THz波段的实验测试示意图。为了确保太赫兹光斑与激光光斑重合,通过实验光路测得太赫兹光斑直径约为3 mm,使用激光显光卡测试得到808 nm激光光斑约为6 mm,调节光路参数保证太赫兹波垂直入射在Ag NPs/CDs调制器中心位置的表面,同时使用808 nm激光器进行调制。808 nm激光作为外部激励源,通过调节激光光斑的位置观察透射系数的变化,从而确保近红外光照射在Ag NPs/CDs与太赫兹波光斑重叠的部分。在近红外激光的调制下,Ag NPs/CDs的表面等离子体特性会极大地改变硅基底的电

导率,从而改变太赫兹波的透过率,实现对太赫兹波的调制。

参考硅基片与Ag NPs/CDs调制器在0.22~0.33 THz波段的太赫兹波传输特性如图3(b)和(c)所示。实验使用808 nm近红外激光照射,激光功率从0 mW逐渐增加到1 086 mW左右,随着激光功率的增加,透射的太赫兹波强度逐渐减小。图3(b)为参考硅基片在不同激光功率下太赫兹波的归一化透射系数,激光功率从10.75 mW逐渐增加到1 086.67 mW,参考硅基片的光生载流子浓度不断增加,导致参考硅基片的透射系数从0.98逐渐减小至0.5附近。图3(c)展示了Ag NPs/CDs调制器在相同激光功率下太赫兹波的归一化透射系数,随着激光功率的增加,Ag NPs/CDs调制器的太赫兹归一化透射系数急剧降低,从0.93降低至0.2附近。对比图3(b)与(c),不难发现Ag NPs/CDs调制器的太赫兹透射系数下降范围远大于相同激光功率下参考硅片太赫兹透射系数的下降范围。这源自于Ag NPs/CDs的表面等离子体共振特性,Ag NPs/CDs会将近红外激光耦合进Ag NPs/CDs的结构中,增强硅基底的光吸收,极大提高了硅基底中光激发载流子的浓度,增加了硅基底的表面电导率,导致了Ag NPs/CDs调制器归一化透射率急剧下降。

为了更直观地显示随着激光功率增加Ag NPs/CDs调制器的太赫兹波衰减情况,利用 $T = T_p / T_0 \cdot 100\%$ 对测得的太赫兹波透射率进行归一化处理。其中, T_p 和 T_0 分别是激光照射时(功率为p)和无激光照射时,Ag NPs/CDs调制器的太赫兹波透射率。图4(a)展示了参考硅片与Ag NPs/CDs的归一化透射光谱,蓝色实线代表了参考硅片而红色实线则代表Ag NPs/CDs,相较于参考硅片,Ag NPs/CDs颗粒的太赫兹透过率随激光功率的增加衰减更加明显。当激光功率达到约1 086 mW时, $T_{Ag\ NPs/CDs}$ 约为17%。在我们之前的工作中曾涉及到相似尺寸的单纯银纳米颗粒调制性能的研究工作^[37],在太赫兹测试实验中,激光功率约为1 W的808 nm近红外光激励下,得到银纳米颗粒的归一化透射率 $T_{Ag\ NPs}$ 约为42%,这表明基于Ag NPs/CDs太赫兹调制器拥有更好的调制性能。调制器的调制性能也可以通过调制深度(MD)来衡量。调制深度定义为 $MD = |T_{on} - T_{off}| / T_{off} \cdot 100\%$,其中 T_{on} 和 T_{off} 分别为有激光照射和无激光照射下通过参考硅片和Ag NPs/CDs调制器的太赫兹波透射率,结果如图4(b)所示。在

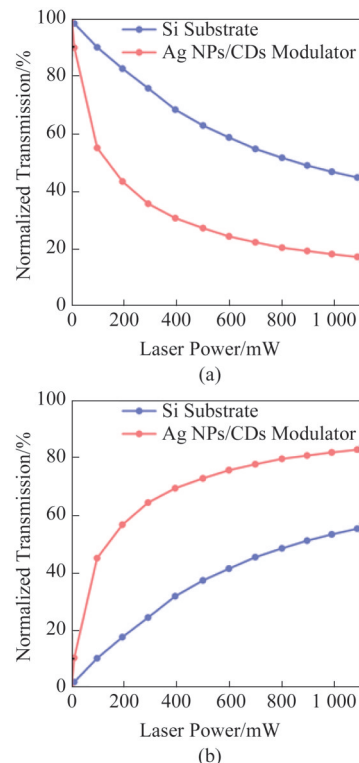


图4 通过参考硅片和Ag NPs/CDs调制器的太赫兹脉冲在不同功率激光照射下的(a)归一化透射率和(b)调制深度

Fig. 4 (a) Normalized transmittance and (b) modulation depth of terahertz pulses through a reference silicon substrate and Ag NPs/CDs modulator under different power laser irradiations

相同功率激光照射下,Ag NPs/CDs调制器的调制深度明显高于参考硅片自身,特别是在较低功率的情况下调制深度增强效果明显;高功率时,调制深度趋于饱和。在功率约为1 086 mW时,Ag NPs/CDs调制器的调制深度约为83%,明显高于参考硅片的调制深度(~54%)。这一结果说明,Ag NPs/CDs能够有效提高太赫兹调制器的调制深度,并且在近红外波段也可以实现太赫兹波调制功能。

3 结论

本文展示了基于银纳米颗粒/碳量子点(Ag NPs/CDs)近红外驱动的太赫兹调制器,利用Ag NPs/CDs结构在硅基底表面制备了Ag NPs/CDs近红外驱动的太赫兹调制器,并对Ag NPs/CDs结构和调制器进行了表征和光控太赫兹波透射特性的实验。结果表明,由于CDs和Ag NPs结合后所具有的量子尺寸效应和介电限域效应,使得Ag NPs/CDs结构可以在近红外波段展现出较好的光吸收特性。在808 nm近红外光的调控下,对Ag NPs/CDs近红外驱动

的太赫兹调制器进行了太赫兹传输特性的测试,结果表明,在0.22~0.33 THz的范围内,Ag NPs/CDs近红外驱动的太赫兹调制器的调制深度可达83%,证明了Ag NPs/CDs太赫兹调制器在近红外波段优异的调制性能,在太赫兹/红外光纤混合通信系统中具有重要应用价值。

References

- [1] Cui N, Guan M, Xu M, et al. High Electric Field-Enhanced Terahertz Metamaterials with Bowtie Triangle Rings: Modeling, Mechanism, and Carbohydrate Antigen 125 Detection [J]. *The Journal of Physical Chemistry C*, 2021, **125**(35): 19374–19381.
- [2] Kleine-ostmann T, Nagatsuma T. A Review on Terahertz Communications Research [J]. *Journal of Infrared, Millimeter and Terahertz Waves*, 2011, **32**(2): 143–171.
- [3] Koenig S, Lopez-diaz D, Antes J, et al. Wireless sub-THz communication system with high data rate [J]. *Nature Photonics*, 2013, **7**(12): 977–981.
- [4] Zhang Zhen-Zhen, FU Zhang-Long, Wang Chang, et al. Research progress on terahertz quantum well detectors [J]. *Journal of Infrared and Millimeter Waves*, 2022, **41**(01) : 103–109.(张真真,符张龙,王长,等。太赫兹量子阱探测器研究进展。*红外与毫米波学报*), 2022, **41**(01) : 103–109.
- [5] Wei Xiao-Dong, Cai Chun-Feng, Zhang Bing-Po, et al. PbTe mid-infrared photovoltage detector [J]. *Journal of Infrared and Millimeter Waves*, 2011, **30**(04) : 293–296.(魏晓东,蔡春峰,张兵坡,等。PbTe中红外光伏探测器。*红外与毫米波学报*), 2011, **30**(04): 293–296.
- [6] LAI W, LIU G, GOU H, et al. Near-IR Light-Tunable Omnidirectional Broadband Terahertz Wave Antireflection Based on a PEDOT: PSS/Graphene Hybrid Coating [J]. *ACS Applied Materials & Interfaces*, 2022, **14** (38) : 43868–76.
- [7] Kleine-ostmann T, Dawson P, Pierz K, et al. Room-temperature operation of an electrically driven terahertz modulator [J]. *Applied physics letters*, 2004, **84**(18) : 3555–7.
- [8] Jakhar A, Kumar P, Moudgil A, et al. Optically Pumped Broadband Terahertz Modulator Based on Nanostructured PtSe₂ Thin Films [J]. *Advanced Optical Materials*, 2020, **8** (7): 1901714.
- [9] Ling Fang, Meng Qing-Long, Huang Ren-Shuai, et al. Multiband modulation characteristics of temperature-controlled terahertz modulators [J]. *Spectroscopy and Spectral Analysis*, 2017, **37**(5): 1334–1338(凌芳,孟庆龙,黄人帅,等。温控太赫兹调制器多频带调制特性。*光谱学与光谱分析*), 2017, **37**(5): 1334–1338
- [10] Li Jia-Bin, Wang Xiao-Hua, Wang Wen-Jie. Mechanistic analysis of terahertz graphene electro-optical modulator based on plasma structure [J]. *Journal of Infrared and Millimeter Waves*, 2021, **40**(2): 143–149.(李佳斌,王晓华,王文杰。基于等离子体结构的太赫兹石墨烯电光调制器的机理分析。*红外与毫米波学报*), 2021, **40** (2): 143–149.
- [11] Lai W, Huang P, Pelaz B, et al. Enhanced All-Optical Modulation of Terahertz Waves on the Basis of Manganese Ferrite Nanoparticles [J]. *The Journal of Physical Chemistry C*, 2017, **121**(39): 21634–21640.
- [12] Lai W, Ge C, Yuan H, et al. NIR Light Driven Terahertz Wave Modulator with a Large Modulation Depth Based on a Silicon-PEDOT:PSS-Perovskite Hybrid System [J]. *Advanced Materials Technologies*, 2020, **5**(4).
- [13] Bai Y, Bu T, Chen K, et al. Review about the optical-controlled terahertz waves modulator [J]. *Applied Spectroscopy Reviews*, 2015, **50**(9): 707–727.
- [14] Reinhard B, Paul O, Rahm M. Metamaterial-based photonic devices for terahertz technology [J]. *IEEE Journal of Selected Topics in Quantum Electronics*, 2012, **19** (1) : 8500912.
- [15] Shi Z W, Cao X X, Wen Q Y, et al. Terahertz modulators based on silicon nanotip array [J]. *Advanced Optical Materials*, 2018, **6**(2): 1700620.
- [16] Hochberg M, Baehr-jones T, Wang G, et al. Terahertz all-optical modulation in a silicon – polymer hybrid system [J]. *Nature Materials*, 2006, **5**(9): 703–709.
- [17] Lee J, Mahendra S, Alvarez P J. Nanomaterials in the construction industry: a review of their applications and environmental health and safety considerations [J]. *ACS nano*, 2010, **4**(7): 3580–3590.
- [18] Wen T, Zhang D, Wen Q, et al. Enhanced Optical Modulation Depth of Terahertz Waves by Self-Assembled Monolayer of Plasmonic Gold Nanoparticles [J]. *Advanced Optical Materials*, 2016, **4**(12): 1974–1980.
- [19] Li Y, Wen T, Zhang D, et al. Comparison Study of Gold Nanorod and Nanoparticle Monolayer Enhanced Optical Terahertz Modulators [J]. *IEEE Transactions on Terahertz Science and Technology*, 2019, **9**(5): 484–490.
- [20] Zhou R, Wang C, Huang Y, et al. Optically enhanced terahertz modulation and sensing in aqueous environment with gold nanorods [J]. *Optics and Lasers in Engineering*, 2020, 133.
- [21] Yu J-P, Chen S, Fan F, et al. Accelerating terahertz all-optical modulation by hot carriers effects of silver nanorods in PVA film [J]. *AIP Advances*, 2019, **9**(7).
- [22] Lai W, Zhu Q, Liu G, et al. Broadband and large-depth terahertz modulation by self-assemble monolayer silver nanoparticle arrays [J]. *Journal of Physics D: Applied Physics*, 2022, **55**(50).
- [23] Gao Y, Wu Y, Huang P, et al. Carbon Dot-Encapsulated Plasmonic Core-Satellite Nanoprobes for Sensitive Detection of Cancer Biomarkers via Dual-Mode Colorimetric and Fluorometric Immunoassay [J]. *ACS Applied Nano Materials*, 2022, **5**(8): 11539–11548.
- [24] Geng B, Hu J, Li Y, et al. Near-infrared phosphorescent carbon dots for sonodynamic precision tumor therapy [J]. *Nature Communication*, 2022, **13**(1): 5735.
- [25] Atabaev T S. Doped Carbon Dots for Sensing and Bioimaging Applications: A Minireview [J]. *Nanomaterials (Basel)*, 2018, **8**(5).
- [26] Choi H, Ko S-J, Choi Y, et al. Versatile surface plasmon resonance of carbon-dot-supported silver nanoparticles in polymer optoelectronic devices [J]. *Nature Photonics*, 2013, **7**(9): 732–738.
- [27] Li X, Rui M, Song J, et al. Carbon and Graphene Quan-

- tum Dots for Optoelectronic and Energy Devices: A Review [J]. *Advanced Functional Materials*, 2015, **25**(31): 4929–4947.
- [28] Dong Y, Yu R, Zhao B, et al. Revival of Insulating Polyethylenimine by Creatively Carbonizing with Perylene into Highly Crystallized Carbon Dots as the Cathode Interlayer for High-Performance Organic Solar Cells [J]. *ACS applied materials & interfaces*, 2022, **14**(1): 1280–1289.
- [29] Vallan L, Imahori H. Citric Acid-Based Carbon Dots and Their Application in Energy Conversion [J]. *ACS applied electronic materials*, 2022, **4**(9): 4231–4257.
- [30] Jiang X, Jin H, Sun Y, et al. Colorimetric and fluorometric dual-channel ratiometric determination of fungicide cy-moxanil based on analyte-induced aggregation of silver nanoparticles and dually emitting carbon dots [J]. *Mikrochim Acta*, 2019, **186**(8): 580.
- [31] Li N, Liu T, Liu S G, et al. Visible and fluorescent detection of melamine in raw milk with one-step synthesized silver nanoparticles using carbon dots as the reductant and stabilizer [J]. *Sensors and Actuators B: Chemical*, 2017, **248**: 597–604.
- [32] Liu S G, Mo S, Han L, et al. Oxidation etching induced dual-signal response of carbon dots/silver nanoparticles system for ratiometric optical sensing of H₂O₂ and H₂O₂-related bioanalysis [J]. *Analytica chimica acta*, 2019, **1055**: 81–89.
- [33] Wei X, Cheng F, Yao Y, et al. Facile synthesis of a carbon dots and silver nanoparticles (CDs/AgNPs) composite for antibacterial application [J]. *RSC advances*, 2021, **11**(30): 18417–18422.
- [34] Yang W, Zhang G, Ni J, et al. Metal-enhanced fluorometric formaldehyde assay based on the use of in-situ grown silver nanoparticles on silica-encapsulated carbon dots [J]. *Mikrochim Acta*, 2020, **187**(2): 137.
- [35] Zhou Q, Liu Y, Wu Y, et al. Measurement of mercury with highly selective fluorescent chemoprobe by carbon dots and silver nanoparticles [J]. *Chemosphere*, 2021, **274**: 129959.
- [36] Sahu B, Kurrey R, Khalkho B R, et al. α -Cyclodextrin functionalized silver nanoparticles as colorimetric sensor for micro extraction and trace level detection of chlorpyrifos pesticide in fruits and vegetables [J]. *Colloids and Surfaces A: Physicochemical and Engineering Aspects*, 2022, 654.
- [37] Takagahara T. Effects of dielectric confinement and electron-hole exchange interaction on excitonic states in semiconductor quantum dots [J]. *Physical review. B, Condensed matter*, 1993, **47**(8): 4569–4584.
- [38] Yue Lan-Ping, HE Yi-Zhing. Absorption spectroscopic study of germanium nanoparticle mosaic films [J]. *Journal of Optics*, 1997(12): 94–97.(岳兰平,何怡贞.纳米锗颗粒镶嵌薄膜的吸收光谱研究[J].光学学报), 1997(12): 94–97.
- [39] Yu Bao-Long, Wu Xiao-Chun, Zou Bing-Lock, et al. Effect of dielectric domain-limiting effect on the optical properties of SnO₂ nanoparticles [J]. *Journal of Physical Chemistry*, 1994(2): 103–106.(余保龙,吴晓春,邹炳锁,等。介电限域效应对SnO₂纳米微粒光学特性的影响。物理化学学报), 1994(2): 103–106.
- [40] Chalopin Yann, Hayoun Marc, Volz Sebastian, et al. Surface enhanced infrared absorption in dielectric thin films with ultra-strong confinement effects [J]. *Applied Physics Letters*, 2014, **104**, 011905.
- [41] Rodina A. V, Efros Al L. Effect of dielectric confinement on optical properties of colloidal nanostructures [J]. *Journal of Experimental and Theoretical Physics*, 2016, **122**(3): 554 – 566.
- [42] Shaganov I I, Perova T S, Melnikov V A, et al. Size Effect on the Infrared Spectra of Condensed Media under Conditions of 1D, 2D, and 3D Dielectric Confinement [J]. *The Journal of Physical Chemistry C*, 2010, **114**(39): 16071 – 16081.
- [43] Lai W., Mazin Abdulmunem O., del Pino P., et al. Enhanced Terahertz Radiation Generation of Photoconductive Antennas Based on Manganese Ferrite Nanoparticles [J]. *Scientific Reports*, 2017, **7**(1): 1–7.